Electronic Supplementary Material (ESI) for Nanoscale.

Supporting Information

Bioinspired Porous-Designed Hydrogel@Polyurethane Sponge Piezoresistive Sensor for Human–Machine Interfacing

Junhao Shen,[a] Yixin Guo,[a,b] Shaohua Zuo,[a,b,*] Fuwen Shi,[a,b,*] Jinchun Jiang,[a,b] Junhao Chu[a,b]

[a]School of Physics and Electronic Science, East China Normal University, Shanghai 200241, China

[b]Engineering Research Center of Nanoelectronic Integration and Advanced Equipment, Ministry of Education

*Corresponding authors

Emails: shzuo@ee.ecnu.edu.cn (SZ), fwshi@ee.ecnu.edu.cn (FS)

Table S1. Raw materials (with their prices) used in fabricating hydrogel@PU sponges.

Materials	Specification	Price [yuan RMB]	Price [dollar U.S.]
Hydrophilic PU sponge	10×8×2 cm^3	5	0.76
Polyvinyl alcohol	500 g	87	13.29
Glycerin	500 mL	51	7.79
Sodium chloride	500 g	24.8	3.79
Hydrogel@PU Sponge	**1 cm^3**	**0.06**	**0.0092**

Table S1 lists the raw materials (with their prices) employed in the preparation of the hydrogel@PU conductive sponges. For actual application, 10 g PVA/glycerol/NaCl solution can be used to prepare 10 conductive sponge samples. The fabrication cost of the conductive sponge was calculated to be ~0.06 yuan RMB, which is approximately 0.0092 US$. In addition, all materials used are biocompatible. This low-cost, biocompatible, flexible piezoresistive sensor has a wide range of application prospects.

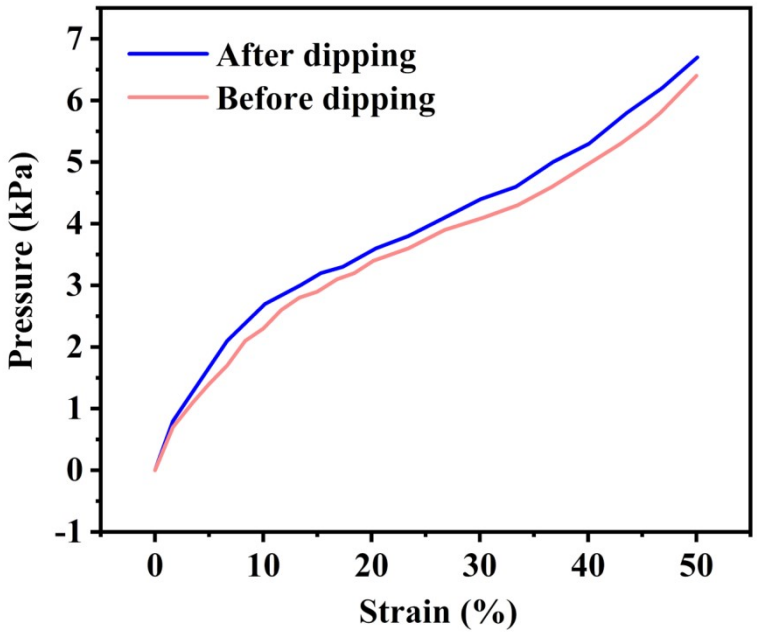

Figure S1. Stress–strain curves of PU sponge and hydrogel@PU sponge in elastic zone and platform zone.

According to **Figure S1**, at 0–10% strain, the compressive modulus of neat sponge and hydrogel@PU sponge were 22.1 kPa and 25.9 kPa. At 10–50%, the compressive modulus of the pure PU sponge was 8.6 kPa. After coating, the compressive modulus of the composite sponge was 9.5 kPa, which is equivalent to the elastic modulus of human soft tissue.[1]

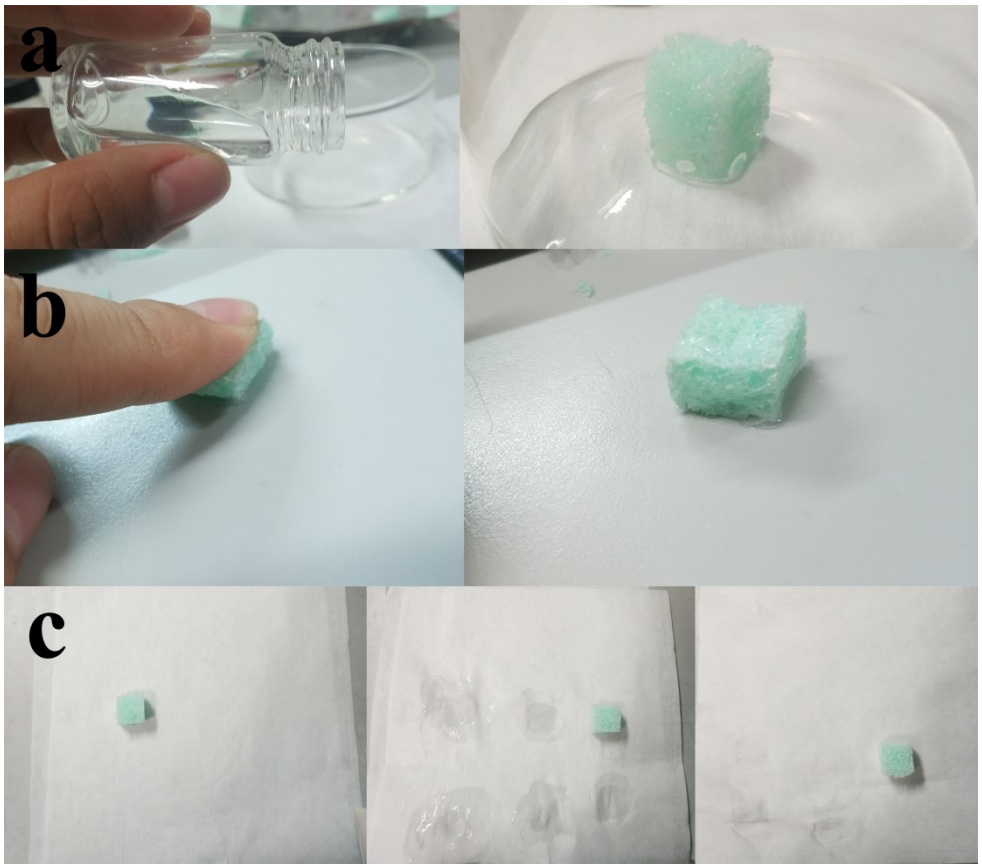

Figure S2. Schematic diagram of sponge coating process.

During the transition from the solution to the hydrogel, the solution always maintains fluidity, and the excess hydrogel solution remaining may flow to the bottom of the sponge (**Figure S2**a). The three components of PVA/glycerin/sodium chloride all have good water retention, and the volume of the formed hydrogel is not much different from that of the solution. Excessive filling of the sponge substrate affects the compressibility of the sensor and brings serious plasticity (Figure S2b). Due to the hydrophilicity of the polyurethane sponge and the excellent adhesion of the hydrogel, we squeeze out the excess solution to form a thin hydrogel coating on the sponge substrate. Continue to squeeze out the hydrogel solution until the sponge can no longer be squeezed out of the exudate on the dust-free cloth (Figure S2c).

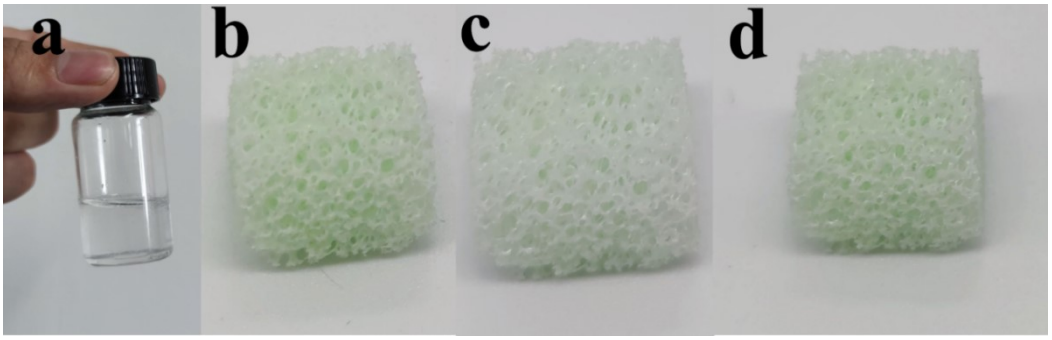

Figure S3. a) PVA/Gl/NaCl solution. Different states of PU sponge: before dipping (a), after dipping (b), and after drying (c).

The PVA/Gl/NaCl solution (4% NaCl) exhibited high transparency (**Figure S3**a). During the dip-coating process into the PVA/Gl/NaCl solution, the hydrophilic PU sponge exhibited water swelling. After drying, the PU sponge became lighter in color. The hardness of the sponge also increased slightly.

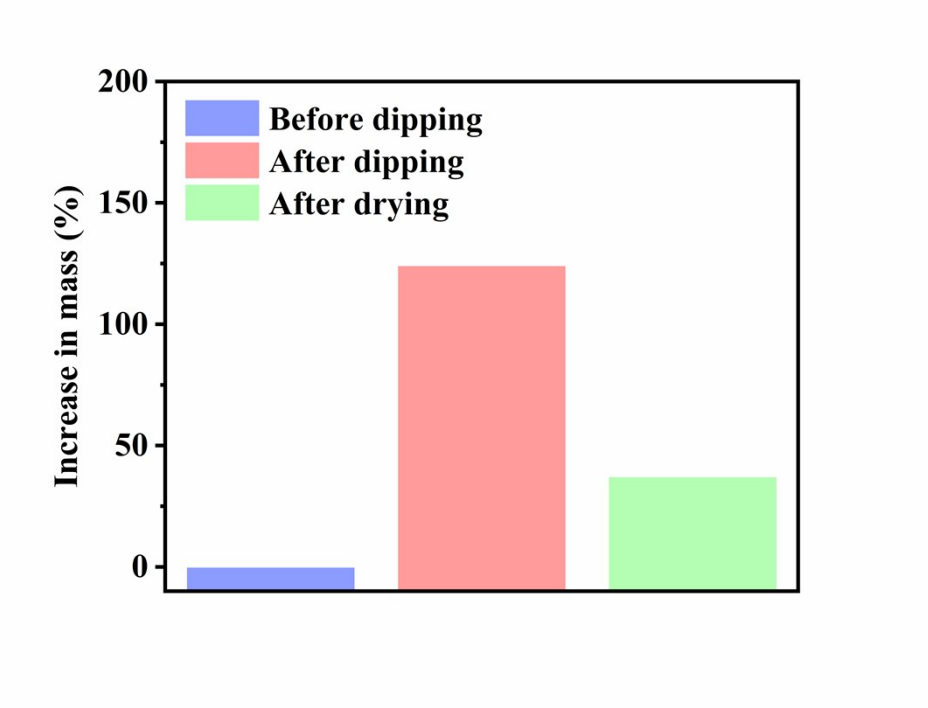

Figure S4. Relative mass change of sponge during preparation.

The neat PU sponge was cut into cubes, each with a volume of 1 cm^3. The PU sponge cube was dipped into and coated with a PVA/Gl/NaCl solution. The excess solution in the sponge was squeezed out. As shown in **Figure S4,** the mass increased by 124% after sponge dipping. After drying at a constant temperature of 25°C (50%RH) for 8 h, the properties of the hydrogel@PU sponge tended to be stable. Compared with that of the neat PU sponge, the mass of the hydrogel@PU sponge increased by 37.2%.

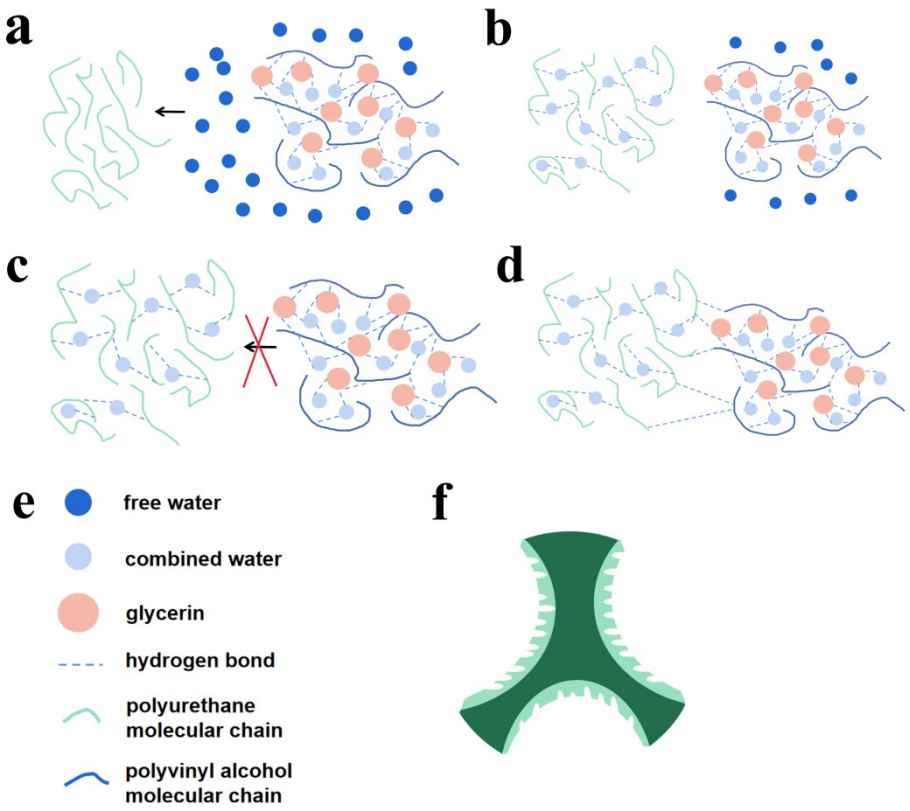

Figure S5. Schematic diagram of the formation process of the hydrogel conductive layer.

As shown in **Figure S5**a and S5b, the swelling phenomenon of the polyurethane sponge may be related to the diffusion of free water molecules in the PVA/glycerol/sodium chloride solution, but after drying, the free water molecules are removed. The hydrolyzed polyvinyl alcohol exhibits the characteristics of being rich in hydroxyl groups, which will generate strong hydrogen bonding force with water molecules and glycerol molecules, and may not be able to diffuse into the interior of the polyurethane sponge(Figure S5c). In the drying process, the adhesive layer and the polyurethane surface are combined by hydrogen bonding to achieve good adhesion (Figure S5d and S5f).

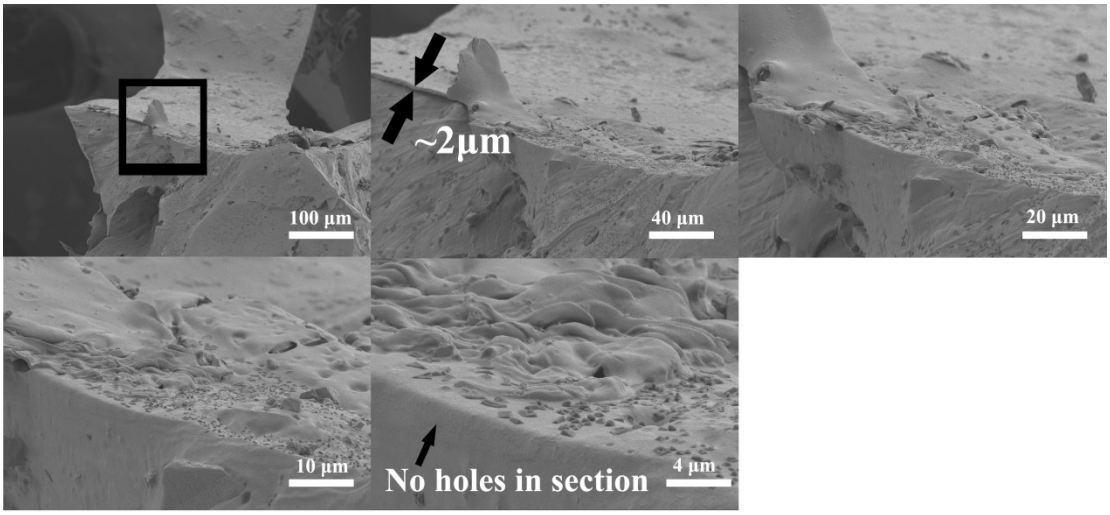

Figure S6. SEM image of the cross-section of the hydrogel @PU sponge.

As shown in the SEM image of the cross-section of the polyurethane coated with hydrogel, the hydrogel layer on the surface is about 2 μm, while no obvious micro-scale pores are found in the polyurethane (near the hydrogel coating layer). The hydrogel layer has almost no effect on the polyurethane substrate.

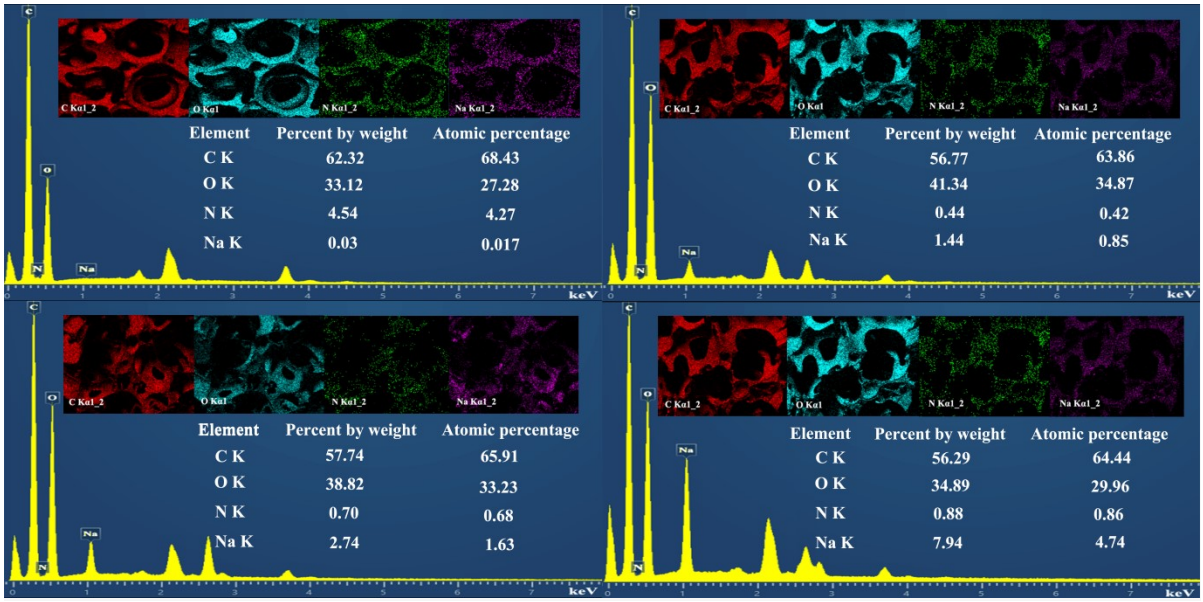

Figure S7. EDS elemental analysis and Mapping analysis of Hydrogel@PU obtained by impregnating PVA/Gl/NaCl electrolyte at different concentrations: (a) 0 wt% NaCl, (b) 2 wt% NaCl, (c) 4 wt% NaCl, and (d) 6 wt% NaCl.

Polyurethane sponge contains nitrogen elements. After the hydrogel layer is coated, the ratio of nitrogen elements decreases, which proves that the hydrogel layer is applied to the sponge substrate. In addition, the specific gravity of sodium in the conductive layer increases as the concentration of sodium chloride increases, and it shows good coating uniformity.

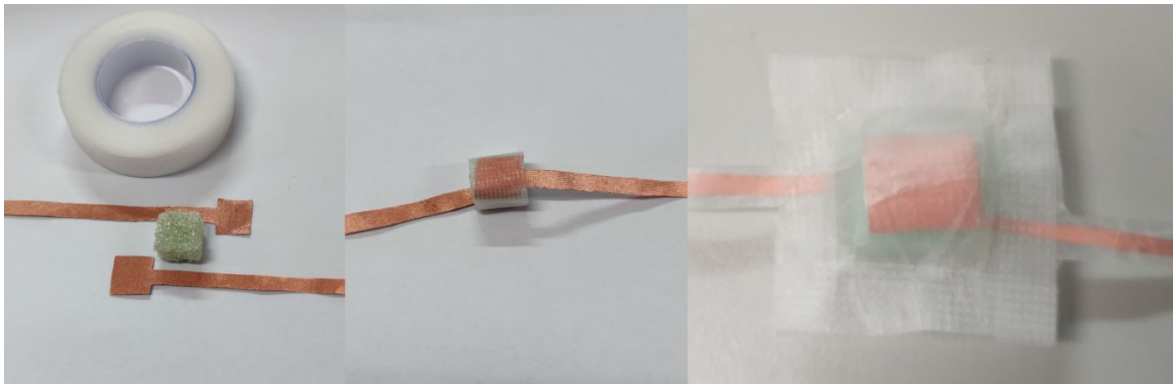

Figure S8. Piezoresistive pressure sensor based on hydrogel@PU sponge.

The piezoresistive pressure sensor was prepared via encapsulation of a hydrogel@PU sponge and conductive copper cloths in medical tape. Both sides of the sponge were coated with conductive silver paste to eliminate contact resistance. Parafilm sealing film was used to encapsulate the sensor to reduce the impact of humidity on the sensor.

Table S2. The conductivity of hydrogel@PU sponges.

Polyvinyl alcohol	Glycerin	Deionized water	Sodium chloride	Conductivity(S/m)
1 g	0 g	8 g	0	8.3×10^{-7}
1 g	1 g	7.8 g	0.2g	1.84×10^{-4}
1 g	1 g	7.6 g	0.4 g	2.96×10^{-4}
1 g	1 g	7.4 g	0.6 g	4.32×10^{-4}
1 g	1 g	7.2 g	0.8 g	6.74×10^{-4}

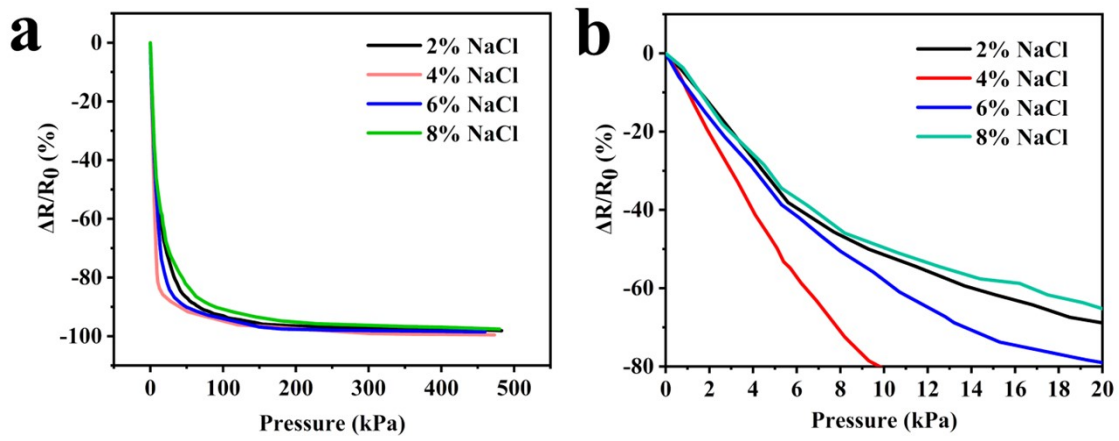

Figure S9. Comparison of sensitivities of hydrogel@PU sponges at different sodium chloride concentrations.

According to **Figure S9**, the sponge dip-coated in the hydrogel solution containing 4% NaCl had the highest sensitivity and that it exhibited linear change in $\Delta R/R_0$ in the range 0–10 kPa. The low addition of NaCl resulted in a low concentration of conductive ions, which affected the conductivity of the coating. On the other hand, high addition of NaCl enhanced the salting-out effect, and excessive chain entanglement resulted in high mechanical strength of the conductive sponge,[2] thereby reducing the sensitivity of the conductive sponge. To obtain the highest sensitivity and a relatively linear pressure detection range, conductive sponges with an addition of 4% NaCl were used during the experiment.

Table S3. Performance comparison of conductive-material-coated sponges.

Material	Preparation method	Sensitivity	Stability	Refs
Graphene@PU	Dipping into GO solution and reduction; Hydrothermal	$\Delta R/R_0$: 0.26 kPa^{-1} (0–2 kPa); 0.03 kPa^{-1} (2–10 kPa)	10000 (2 kPa pressure)	3
MXene@CS@PU **(crack-designed)**	Dip coating	$\Delta R/R_0$: 0.014kPa^{-1} (0–6.5 kPa); −0.015 kPa^{-1} (6.5–85.1 kPa); −0.001 kPa^{-1} (>85.1 kPa) GF : 0.17 (0–30% strain); −0.23 (30–45% strain); −3.0 (45–85% strain)	10000 (0–20% strain)	4
Gold@PU **(crack-designed)**	Sputtering	$\Delta R/R_0$: 0.059kPa^{-1} (0–4.7 kPa); −0.096 kPa^{-1} (4.7–10.2 kPa); −0.122 kPa^{-1} (10.2–14.2 kPa) GF : 1.09 (0–23% strain); −1.34 (0–47% strain); −4.43 (47–60% strain)	1000 (0–45% strain)	5
CNT/rGO@PU **(crack-designed)**	Dip coating	$\Delta R/R_0$: 0.022 kPa^{-1} (0–2.7 kPa); −0.088 kPa^{-1} (2.7–10.8 kPa); −0.034 kPa^{-1} (10.8–48.8 kPa)	5000 (0–50% strain)	6

		GF : 0.051 (0–50% strain); −2.13 (50–86% strain); −2.3 (86–98% strain)		
Carbon black@PU **(crack-designed)**	Layer-by-layer assembly (alternatively coating)	$\Delta R/R_0$: 0.068 kPa^{-1} (0–2.3 kPa); −0.023 kPa^{-1} (2.3–10 kPa); −0.036 kPa^{-1} (10–16kPa) GF : 2.2 (0–10% strain); −0.38 (10–50% strain); −3.1 (50–60% strain)	50000 (0–40% strain)	7
Gellulose nanofibril/AgNWs@PU **(crack-designed)**	Dip coating	GF : 26.07 (0–0.6% strain); −5.71 to −0.52 (0.6–70% strain); −0.13 (70–80% strain)	500 (0–40% strain)	8
rGO@PU	Dip coating	R/R_0 : 0.67 kPa^{-1} (0–1.5 kPa); 0.04 kPa^{-1} (1.5–30 kPa)	100 (0–70% strain)	9
PEDOT:PSS@Melamine	Dip coating	GF : −1.10±0.03 to −2.32±0.41 (0–88.1±2.2% strain)	1000 (10–30% strain)	10
rGO-CB@loofah	Reduction and self-assembly	$\Delta I/I_0$: 0.66 kPa^{-1} (0–0.5 kPa); 1.89 kPa^{-1} (0.5–2.0 kPa)	5000	11
Graphene@PDMS	Dip coating	GF : −8.77 (0–9.5% strain);	36000	12

		−8.77 to −2 (9.5–50% strain)	(0–5% strain)	
CNTs@PDMS	Dip coating	GF : −5.6 (0–2.5% strain); −1.16 (2.5–60% strain)	255 (0–60% strain)	13
Hydrogel@PU (porous-designed)	**Dip coating once**	**$\Delta R/R_0$: −0.083 kPa^{-1} (100 Pa to 10.0 kPa); −0.051 kPa^{-1} (10.0–123.3 kPa); −0.0001 kpa^{-1} (123.3–470.2 kPa) GF : −1.33 (1–60% strain); −0.57 (60–93% strain)**	**10000 (0–80% strain)**	**This work**

Table S3 lists the materials and properties of conductive coating sponges as reported in recent years. Conductive sponges based on crack design have inflection points in their sensitivity and GF curves, which are limited in actual signal detection. Most conductive voltage resistance sensors based on brittle conductive materials have high sensitivity and limited pressure detection ranges (<100 kPa). When the sensors are subjected to 0–60% compression (wherein the stress and strain of the PU sponge are almost linear), the changes in GF are often regional rather than continuous. This is because of the asynchronous compression of the conductive coating and sponge skeleton; the rigid conductive coating is not compressible. By contrast, when the strain is greater than 60%, the PU sponge substrate usually becomes dense. The

sponge skeletons contact and squeeze each other, resulting in the restriction of further compression of the sponge. Nonetheless, the extrusion of the sponge skeleton and incompressibility of the coating result in more conductive contacts.

In accordance with $GF=(\Delta R/R_0)/strain$, the GFs of traditional conductive material-coated sponges increase under large strains. Unfortunately, such high performance is considered inconsequential for these sensors. At large strains, traditional conductive coating materials undergo plastic deformation or fracture because of their brittleness and incompressibility. Continuous loading and unloading under large strains exacerbate the instability of such coatings. This is why the reported cycling stability tests of conductive coating sponges were all performed in the elastic zone (0–20%) and platform zone (20–60%). By contrast, hydrogel@PU conductive sponges have a wide range of pressure detection and high compressibility because of the high toughness of the conductive coating and the compressibility of the porous structure of the coating. The porous hydrogel coating and sponge skeleton can be compressed simultaneously, which provides hydrogel@PU sponges with good cyclic stability at large strains.

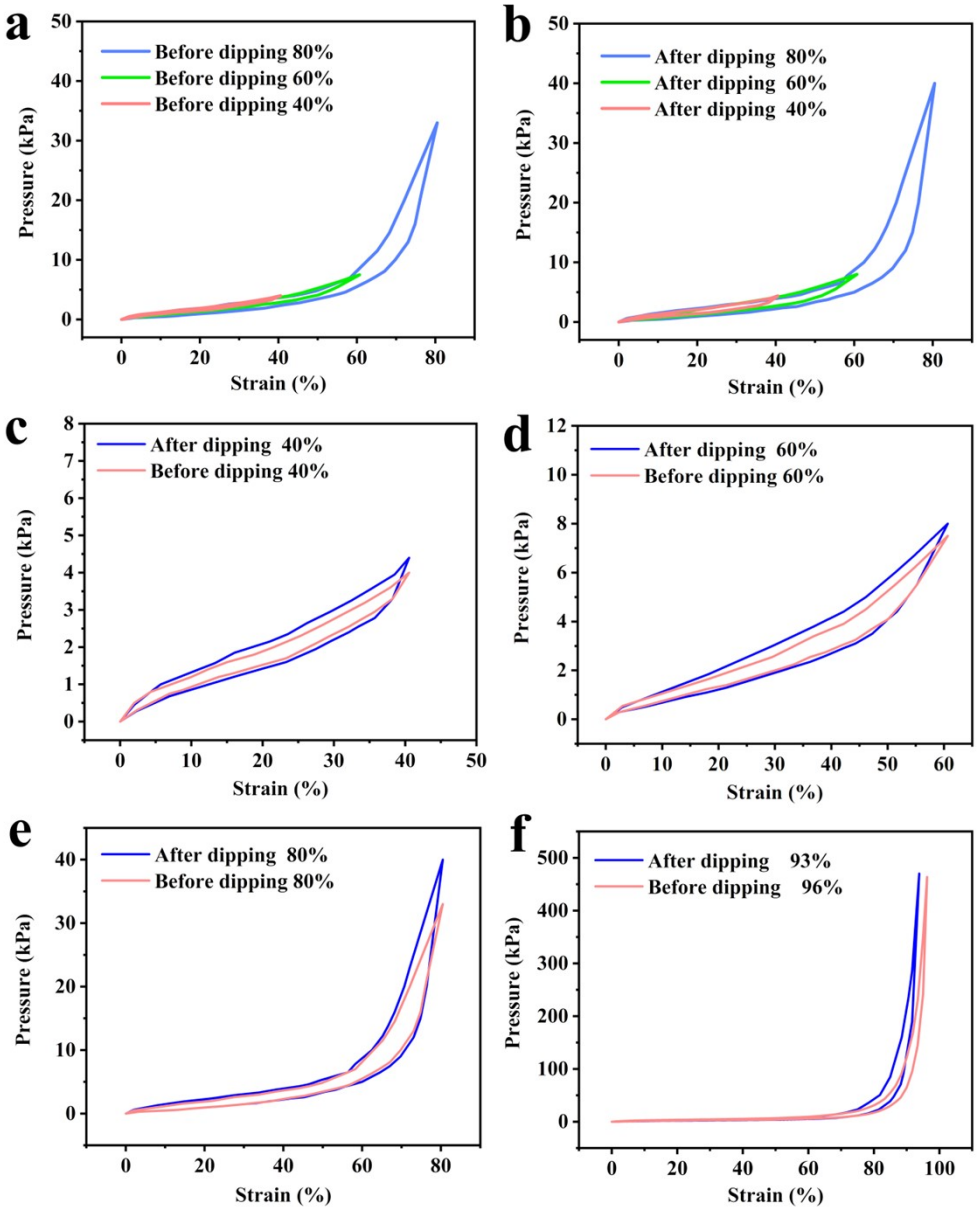

Figure S10. Stress–strain curve of hydrogel@PU sponge at different compression conditions.

As shown in **Figure S10**a, the neat PU exhibited a typical stress–strain curve of a polymer elastomer sponge. In the elastic zone (0–20.0% strain), the compressive stress of the PU sponge increased linearly. In the platform area (20.0–60.0% strain), the compressive stress of the PU sponge increased slowly. The stress values of the PU sponge at 40.0% and 60.0% compression were 4.0 kPa and 7.5 kPa, respectively

(**Figures S10**c, d). When the strain was higher than 60.0%, most of the sponge skeleton achieved operational contact, and further compression led to a higher stress increase. At 80.0% strain, the stress was 33 kPa (**Figure S10**e). Further to the maximum compression 96%, the stress was 463.0 kPa. On the other hand, the stress–strain curve of the prepared hydrogel@PU sponge is similar to that of the pure PU sponge (**Figure S10**b), which indicates that the hydrogel@PU sponge has similar mechanical properties. At 40%, 60%, and 80% strain, the corresponding pressures were 4.4, 9.5, and 40.1 kPa (**Figures S10**c–e). The maximum compression of the hydrogel@PU sponge was measured to be 93%, which corresponded to a stress of 470.2 kPa (**Figure S10**f). The pressure–strain curve of the neat PU sponge shows evidence of hysteresis.

During the compression and release of the PU sponge, hydrogen bonds in the urea phase segments were broken and rearranged. This energy dissipation mechanism resulted in the hysteresis of the PU sponge. In addition, as the applied strain increased, the hysteresis became more pronounced (**Figures S10**c–f). At 40%, 60%, 80%, and 96% compression, the hysteresis factors of the pure PU sponge were 16.4%, 19.2%, 27.4%, and 35.5%, respectively. In contrast, when the hydrogel@PU sponge was subjected to 40%, 60%, 80%, and 93% compression, the hysteresis factors were 23.3%, 25.8%, 33.6%, and 41%, respectively (**Figures S10**c–f). The coating of the tough hydrogel increased the hysteresis of the PU sponge because of the addition of sacrificial bonds (hydrogen bonds), which may increase the recovery time of the sensor.

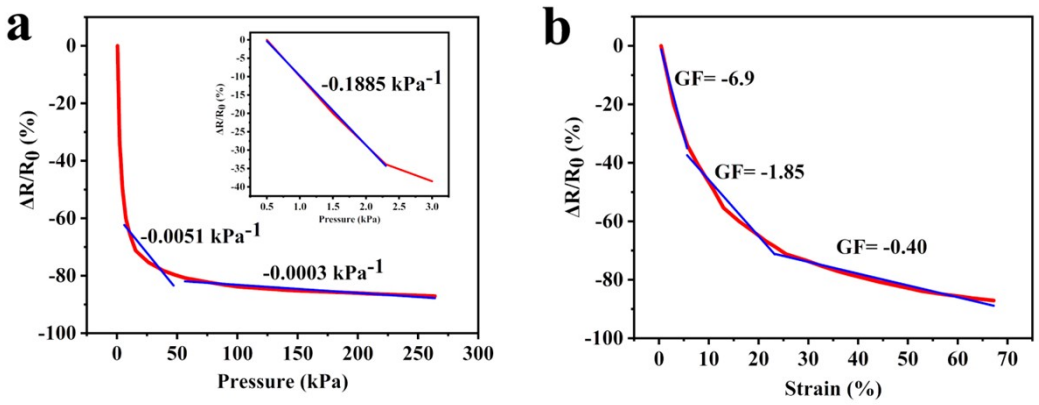

Figure S11. Sensitivity and GF of PVA/Gl/NaCl hydrogel.

Through a combination of 1 g of glycerol, 0.4 g of NaCl, and 8.6 g of PVA solution (PVA : deionized water = 1:7.6), the PVA/Gl/NaCl solution was prepared. The solution was dried at room temperature for 24 h to form a PVA/Gl/NaCl hydrogel. As shown in Figure S11, the PVA/Gl/NaCl hydrogel exhibited a high sensitivity of −0.1885 kPa^{-1} (0–2.3 kPa) and a high GF of −6.9 (0–6% strain). However, tough hydrogels are rarely used as compressive stress sensors because of their limited compressibility (small pore size and small porosity) and fatigue damage.

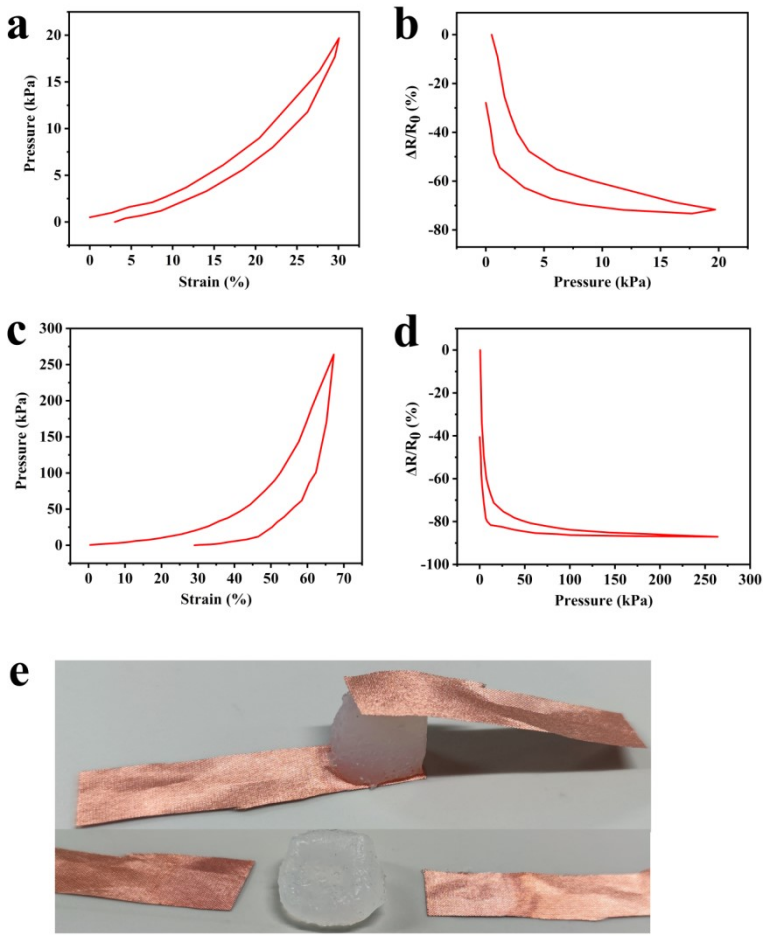

Figure S12. Effect of fatigue on PVA/Gl/NaCl hydrogel under different compression conditions.

The PVA/Gl/NaCl hydrogel exhibited obvious fatigue damage. The hydrogel was cut into small 1-cm pieces for the piezoresistance test. The continuous loading time was 1 min. During the loading and unloading process at 0–30% strain, the hydrogel exhibited a 3% loss of height, and the resistance reduced to 72.2% of the initial value. The height and resistance of the hydrogel returned to their initial values within 5 h. Subjected to a strain load of 65%, the hydrogel underwent plastic deformation. The

height of the hydrogel was permanently decreased by 29.0%, and the resistance value reduced to 40.5% of the initial value.

The PVA/Gl/NaCl hydrogel has a large number of sacrificial bonds. High toughness is obtained through fracture and reorganization of these sacrificial bonds. However, the large number of sacrificial bonds lead to inevitable effects of fatigue on these hydrogels, which limit the application of tough hydrogels in compressive stress sensing.

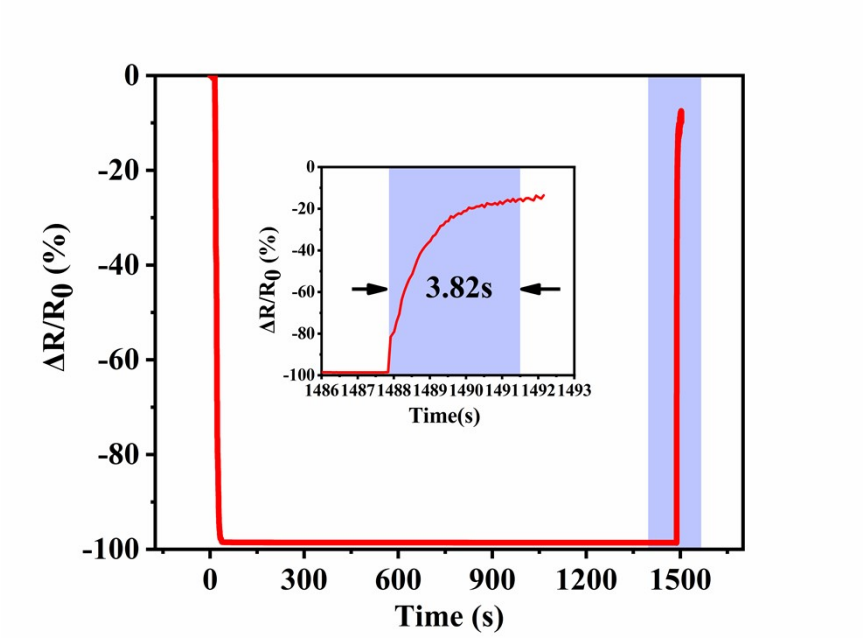

Figure S13. Recovery time of hydrogel@PU sponge subjected to continuous large strain loading.

As shown in **Figure S13,** a hydrogel@PU sponge was unloaded after being continuously loaded for 1500 s at 90% strain. The electrical resistance of the hydrogel@PU sponge recovered to 93% of its initial value after 3.82 s. The height of the sponge returned to 98% of its initial value. The conductive sponge did not exhibit plastic deformation, which provides a new application strategy for tough hydrogel materials.

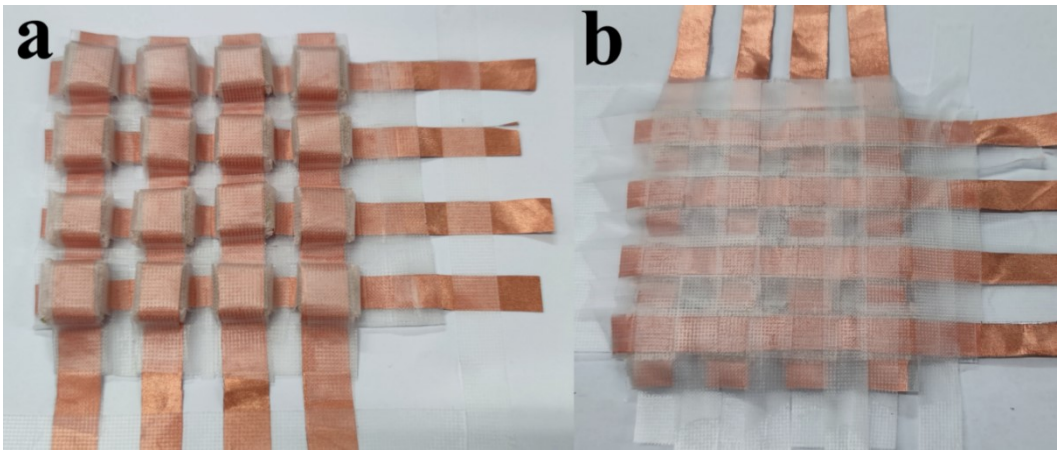

Figure S14. a) Electronic skin based on hydrogel@PU sponge. b) Electronic skin in actual use.

Hydrogel@PU sponges and conductive copper cloths were encapsulated in medical tape to prepare electronic skin. The electronic skin had 16 isolated pixels (**Figure S14**a). In the actual test, the electronic skin was turned upside down and fixed (**Figure S14**b). Pulling between the medical tapes and sponges provided dentability to the electronic skin. The external force was shared by all sponges, which better simulated the sensing mode of the human skin.

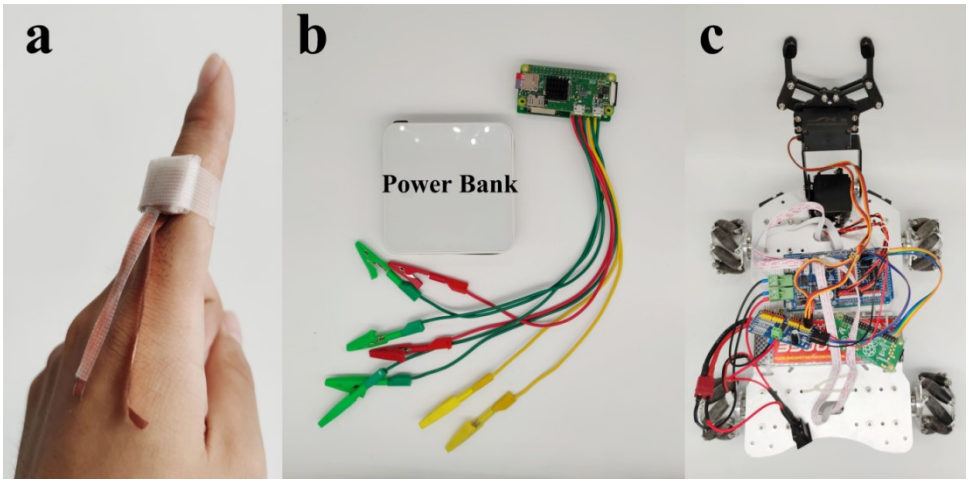

Figure S15. a) Encapsulated sensor. b) Control circuit board powered by a power bank. c) Smart vehicle based on Raspberry Pi.

The 1.5 cm × 1.5 cm × 0.5 cm hydrogel@PU sponge was encapsulated in medical tape (**Figure S15**a). The control circuit had four resistance-detection channels and was powered by a power bank. The control circuit and the smart car were developed using a Raspberry Pi Zero, and they communicated with the computer via Wi-Fi.

References

1 J. B. Weaver, M. Doyley, Y. Cheung, F. Kennedy, E. L. Madsen, E. E. Van Houten and K. Paulsen, *Clin. Biomech.* (Bristol, Avon), 2005, **20**, 312-319.

2 S. Peng, S. Liu, Y. Sun, N. Xiang, X. Jiang and L. Hou, *Eur. Polym. J.*, 2018, **106**, 206-213.

3 H. B. Yao, J. Ge, C. F. Wang, X. Wang, W. Hu, Z. J. Zheng, Y. Ni and S. H. Yu, *Adv. Mater.*, 2013, **25**, 6692-6698.

4 X. P. Li, Y. Li, X. Li, D. Song, P. Min, C. Hu, H. B. Zhang, N. Koratkar and Z. Z. Yu, *J. Colloid Interface Sci.*, 2019, **542**, 54-62.

5 Y. H. Wu, H. Z. Liu, S. Chen, X. C. Dong, P. P. Wang, S. Q. Liu, Y. Lin, Y. Wei and L. Liu, *ACS Appl. Mater. Interfaces*, 2017, **9**, 20098-20105.

6 A. Tewari, S. Gandla, S. Bohm, C. R. McNeill and D. Gupta, *ACS Appl. Mater. Interfaces*, 2018, **10**, 5185-5195.

7 X. Wu, Y. Han, X. Zhang, Z. Zhou and C. Lu, *Adv. Funct. Mater.*, 2016, **26**, 6246-6256.

8 S. Zhang, H. Liu, S. Yang, X. Shi, D. Zhang, C. Shan, L. Mi, C. Liu, C. Shen and Z. Guo, *ACS Appl. Mater. Interfaces*, 2019, **11**, 10922-10932.

9 L. Zhao, F. Qiang, S. W. Dai, S. C. Shen, Y. Z. Huang, N. J. Huang, G. D. Zhang, L. Z. Guan, J. F. Gao, Y. H. Song and L. C. Tang, *Nanoscale*, 2019, **11**, 10229-10238.

10 Y. Ding, J. Yang, C. R. Tolle and Z. Zhu, *ACS Appl. Mater. Interfaces*, 2018, **10**, 16077-16086.

11 D. Sengupta, Y. Pei and A. G. P. Kottapalli, *ACS Appl. Mater. Interfaces*, 2019, **11**, 35201-35211.

12 R. Iglio, S. Mariani, V. Robbiano, L. Strambini and G. Barillaro, *ACS Appl. Mater. Interfaces*, 2018, **10**, 13877-13885.

13 M. Cao, S. Fan, H. Qiu, D. Su, L. Li and J. Su, *ACS Appl. Mater. Interfaces*, 2020, **12**, 36540-36547.